NASA Technical Memorandum 82694
AIAA-81-2049

Turbomachinery Noise Studies of the AiResearch QCGAT Engine with Inflow Control

J. G. McArdle, L. Homyak,
and D. D. Chrulski
Lewis Research Center
Cleveland, Ohio

Prepared for the
Seventh Aeroacoustics Conference
sponsored by the American Institute of
Aeronautics and Astronautics
Palo Alto, California, October 5-7, 1981

NASA

TURBOMACHINERY NOISE STUDIES OF THE AIRESEARCH QCGAT ENGINE WITH INFLOW CONTROL

J. G. McArdle, L. Homyak, and D. D. Cnrulski

National Aeronautics and Space Administration
Lewis Research Center
Cleveland, Ohio 44135

E-977

Abstract

The AiResearch Quiet Clean General Aviation Turbofan (QCGAT) engine was tested on an outdoor test stand to compare the acoustic performance of two inflow control devices (ICD's) of similar design, and three inlet lips of different external shape. Only small performance differences were found. Far-field directivity patterns calculated by applicable existing analyses were compared with the measured tone and broadband patterns. For some of these comparisons, tests were made with an ICD to reduce rotor/inflow disturbance interaction noise, or with the acoustic suppression panels in the inlet or bypass duct covered with aluminum tape to determine "hardwall" acoustic performance. The comparisons showed that the analytical expressions used predict many directivity pattern features and trends, but can deviate in shape from the measured patterns under certain engine operating conditions. Some patterns showed lobes from modes attributable to rotor/engine strut interaction sources.

Introduction

The Quiet Clean General Aviation Turbofan (QCGAT) engines are medium-thrust engines sized for business aircraft. Two distinctly different QCGAT engines were made specially for NASA to demonstrate that technology developed for large commercial and military engines could be successfully adapted to smaller engines. The engines were designed and manufactured by AiResearch Manufacturing Company of Arizona (now the Garrett Turbine Engine Company) and by AVCO Lycoming Division. Each of the engines incorporates many modern design features such as a mixer exhaust nozzle system, low-emission combustors, geared fan, and noise reduction techniques including acoustic suppression panels in the inlet and in the bypass duct.

The present paper deals only with the AiResearch QCGAT engine. After testing at the factory to compare overall performance with design predictions,[1,2] the engine was delivered to NASA Lewis Research Center. It was installed on an outdoor static test stand for acoustic performance tests along with instrumentation to measure aerodynamic and flow parameters useful in analyzing the acoustic data. Many of the tests were performed with an inflow control device (ICD) mounted over the engine inlet to reduce incoming flow disturbances and, consequently, tone noise caused by rotor interaction with these disturbances.

This paper reports results of tests performed for three purposes. The first is to compare the acoustic performance of three inlet lips of different external shape and two available ICD's on the same engine. The two ICD's had the same overall size and shape but differed in some details of the turbulence reducing design approach. In previous test programs with different fans, both of these ICD's significantly reduced fan fundamental blade passing frequency (BPF_F) tone noise from rotor/turbulence interaction.[3,4] The second purpose is to compare the acoustic performance of three inlet lips of different external shape on the same engine. The lips were intended for use with the basic engine inlet and with the two ICD's. The third purpose is to compare far-field directivity patterns calculated by applicable existing analyses with the measured BPF_F and broadband patterns. The comparisons, although qualitative, provide good insight into the engine sources contributing to the far-field noise.

Test results are shown for the engine alone, for the engine with the different inlet lips and ICD's, and for the engine with an ICD and some or all of the acoustic suppression panels covered with aluminum tape to form hardwall ducts. Results generally are presented as far-field spectra or directivity patterns for two engine power settings. Directivity patterns for the engine without an ICD are compared with pattern shapes calculated by simple expressions from existing multimodal analyses. Directivity patterns for the engine with an ICD are searched for evidence of propagating single modes that lead to identification of their sources.

Apparatus

Engine

The QCGAT engine (Fig. 1) has 4.2 bypass ratio and produces about 1800 N (4000 lbs.) thrust at sea-level-static conditions. It is a geared, front-fan, twin-spool configuration. The low-pressure spool consists of a four-stage axial compressor and single-stage, 36-blade fan driven by a three-stage axial turbine. The 77.7 cm (30.6 in.) diameter fan is geared down by a 2.16 ratio planetary system. The high-pressure spool consists of a single-stage centrifugal compressor driven by a single-stage axial turbine. The low-smoke combustor is a reverse-flow annular design with an air assisted fuel nozzle system. The noise reduction features include: no inlet guide vanes, low-tip-speed fan, large fan rotor/stator spacing, vane/blade ratios for acoustic cut-off of BPF_F rotor/stator interaction tones, 12-lobe mixer exhaust nozzle system, and acoustic treatment in the inlet and the aft bypass duct. The treatment consisted of single-degree-of-freedom acoustic suppression panels described in Fig. 2. The panels were designed by the engine manufacturer using methodology described in Ref. 5. For "hardwall" tests, the porous flow-side surfaces of the panels were covered over by aluminum tape to obtain impervious duct walls having the same size and shape.

Inlets - The QCGAT "flight" inlet was designed to meet contract performance goals. The length was set by the length of the acoustic panels needed to meet the fan-noise suppression

goals, and the lip was chosen for low flight drag.[5] For ground testing, the inlet lip was replaced by a thicker "flight simulator" lip as shown in Fig. 3. This lip was the same as the flight lip downstream of the flight highlight. Upstream of the highlight the flight simulator inlet lip was contoured to provide a good match with the flight inlet Mach number gradient near the wall.

In order to mount the available ICD's on this inlet, the flight simulator lip was smoothly extended outward, as sketched in Fig. 3. For ICD No. 1A, the extension consisted of a large conical surface approximately 2.2 fan diameters in size. For ICD No. 1, the same cone was cut back and faired into a cylindrical section 1.38 fan diameters in size.

Inflow control devices - The inflow control devices (ICD's) are shown in Fig. 4. Both of the ICD's had the same overall shape and dimensions, but had two design differences. The first difference was that the turbulence reducing screen was located on the downstream side of the honeycomb for ICD No. 1, whereas the screen was mounted separately 5 cm (2 in.) from the downstream side of the honeycomb for ICD No. 1A. For the latter design, the screen location was intended to give the most effective reduction in axial turbulence velocity.[4] The second difference was the manner in which air entered the ICD from the rear; in ICD No. 1, the air flowed along a cylindrical surface axially into the honeycomb, while in ICD No. 1A, the air entered from a 36-degree conical surface. For ICD No. 1A, the conical surface had been used in another program to reduce rotor/turbulence interaction noise,[4] and the surface was retained because it may have decreased distortions in the flow entering the engine from the rear. Both ICD's were supported by thin rods from an overhead structure (Fig. 4(c)), and in addition ICD No. 1A was held against the conical surface by tie rods back to the engine.

ICD No. 1 was previously used in an outdoor test program with another engine.[3] ICD No. 1A was previously used in a fan test program in an anechoic test chamber.[4] Those tests demonstrated that both ICD's significantly reduced the BPF_F tone from rotor/turbulence interaction, and did not attenuate or redirect the sound passing from the engine to the far field.

Aerodynamic performance characteristics - Fan related aerodynamic performance for the basic engine is shown in Fig. 5. A complete description of engine performance is given in Ref. 1. Engine performance was not changed significantly when an ICD was installed because the pressure drop across the ICD is very small.[3] Corrected fan speeds for "approach" and "takeoff" power are given in Fig. 5. These speeds were selected by the engine manufacturer to represent operation of this engine in a business jet aircraft.

Acoustic performance characteristics - One-third octave directivity patterns for the basic engine without an ICD are presented in Fig. 6. The engine was configured with all acoustic suppression panels installed, and with the panels covered with aluminum tape to form hardwall ducts. The panels reduced the noise throughout the far field at both engine power settings. They were most effective in the aft quadrant at the lower power setting because large panels tuned to frequencies near the BPF_F at that speed (see Fig. 2) were installed in the bypass duct. The panels were least effective at angles near the inlet axis; this result supports the idea that the panels less readily absorb the well-cut-on acoustic modes, which are the modes that tend to propagate near the axis.[6] The noise fell off in the "zone of relative silence," a directivity region which receives little acoustic radiation from the exhaust nozzle due to refraction at the shear layer between the exhaust jet and the ambient air.[7] A complete report of acoustic performance is given in Refs. 1 and 2.

Another way to characterize the engine acoustic performance is by means of far-field noise spectra. Narrowband spectra for this engine at far-field angles of 50 and 110 degrees are shown in Fig. 7. In the spectra the BPF_F tone always stands distinctly above the broadband base because the engine produced much tone from rotor/inflow disturbance interaction, as usually occurs in outdoor tests without an ICD. At low power the acoustic panels suppressed the BPF_F tone as well as the broadband noise through a large range of frequencies around BPF_F (approximately 1000 to 6000 Hz). However, at "take-off" power, the suppression in the same frequency range does not appear to be as large, possibly because of "floors" caused by exhaust system noise. Also, at "take-off" power multiple pure tones are low level, compared to the BPF_F tone, because the fan tip relative Mach number is only slightly above unity. In addition, many of the tones were cut-off in the inlet duct because the cut-off ratio is less at the throat than at the fan face.[8]

Facility

The tests were performed at the NASA LeRC Vertical Lift Fan (VLF) Facility. This facility is an outdoor static test stand equipped to measure engine steady-state aerodynamic and acoustic performance. The photograph in Fig. 1(b) shows the engine mounted for testing at VLF. The engine centerline is 2.9 m (9.5 ft) above the ground. The surface between the engine and the far-field microphones is level concrete.

Instrumentation and Data

Aerodynamic performance was measured by conventional speed, force, pressure, temperature, and other transducers as appropriate. The data were averaged over approximately 30 seconds of engine run time, then plotted to describe the performance characteristics.

Acoustic performance was measured by far-field ground microphones on a 24.4-m (80-ft) radius circle, and by wall transducers in the inlet duct. The one-third-octave far-field data were corrected to free-field, 30.5-m (100-ft) radius, standard-day conditions by a computer program. The sound pressure level (SPL) correction from ground microphones to free field was -6.0 dB. The same corrections were applied to SPL values read from narrowband spectra obtained from fast Fourier transforms of 25-second samples of the recorded data.

When BPF_F tone and broadband data are shown on the same figure, the broadband results were obtained by drawing the broadband line through the base of the tone on narrowband SPL plots. Thus, the broadband results are determined by the SPL measured at frequencies either side of BPF_F and are intended to represent the level that would have been measured if there had been no BPF_F tone at that location.

When an engine configuration was tested both with and without an ICD, both datasets usually were obtained in the same test session in order to minimize possible differences caused by variations in weather or hardware assembly.

Results and Discussion

In this section the calculated fan speeds for acoustic cut-off in the QCGAT engine are shown, and the circumferential mode numbers for single modes most likely to be produced in testing are identified. The effects of three inlet lip shapes and two ICD's on the acoustic performance of the engine are then shown. Results are presented as acoustic spectra or far-field directivity patterns. Then the BPF_F tone and broadband directivity patterns without an ICD are compared with forward and aft patterns calculated by existing multimodal analyses. Finally, for tests with an ICD to minimize rotor/inflow disturbance interaction noise, the forward patterns are examined for evidence of propagating single modes that leads to identification of their sources.

Cut-Off Speeds

The corrected fan speeds at which spinning acoustic modes at BPF_F become cut-off or cut-on (i.e., unity cut-off ratios per Tyler-Sofrin theory as discussed in Ref. 8), in this engine are shown in Fig. 8(a). For speeds higher than cut-off speed modes are cut-on and propagate, while for lower speeds modes are cut-off and tend to decay. For the inlet the speeds were calculated using the measured airflow, and are shown for cut-off at the fan face and at the inlet throat. Tones which are cut-on at the fan face can be cut-off at the throat because the throat in this inlet is 0.83 fan diameters.

The tests reported in Ref. 3 showed that propagating modes at BPF_F could be produced by rotor interaction with distortions from ICD ribs and from engine struts aft of the fan in the bypass flow duct. On the basis of those results and as illustrated in Fig. 8(b), for BPF_F tones the modes most likely to be formed during these tests are circumferential mode numbers 36 (rotor alone), 28, 20, 12, and 4 (rotor interaction with 8 structural struts in the bypass duct), and 24 and 12 (rotor interaction with 12 ribs in the ICD, which always was mounted with ribs on the engine vertical and horizontal centerlines). No propagating modes from rotor/vane interaction are expected becasuse of high vane/blade ratios in both the core and bypass flow passages. Also, no propagating modes of interest are expected from rotor interaction with the 10 structural struts in the core duct because those modes are cut-off in the small duct diameter.

At the mixer exhaust nozzle exit, cut-off was computed from measured airflow and thrust, assuming ambient pressure at the exit plane and perfect core and bypass flow mixing with the 12-lobe nozzle. For this engine the speed at which modes become cut-on at the nozzle is higher than at the fan; therefore, some spinning modes propagating from the fan may not radiate to the far field because they are cut-off at the nozzle exit. Some computations were performed to determine if modes cut-on at the fan even could propagate through the bypass duct to the nozzle. It was found that modes cut-on at the fan face at "approach" power are also cut-on in the duct to the nozzle exit, but modes near cut-off at "takeoff" power can become cut-off in the bypass duct ahead of the nozzle. The latter effect occurs because the lower flow velocity and higher gas temperature both tend to reduce duct flow Mach number (compared to the fan face) and, therefore, cut-off ratio in the passage at stations where the outside diameter is nearly the same as the fan. In addition, possible effects of the two engine pylons and 12-lobe mixer nozzle on duct propagation are unknown, and are ignored in these calculations.

Acoustic Performance

Effect of lip shape on forward noise - The same inlet could be fitted with three lips (see Fig. 3) which differed in shape and size outside the highlight only. All the lips were relatively "thick" like a bellmouth, and thus were not expected to change the inflow or the source noise significantly. In addition, the lip shape changes were not expected to alter the forward directivity pattern because external changes theoretically affect only the pattern near sideline angles (near 90 deg.), as discussed in Refs. 9 and 10.

A test with each lip was made with no ICD, a hardwall inlet duct, and all acoustic panels in the bypass duct so that results would emphasize any changes in inlet directivity due to the lip. The forward quadrant BPF_F and broadband directivity patterns measured in these tests are given in Fig. 9. As expected, there was little difference in the patterns for all these lips, except in tone level near the sideline.

Effect of ICD - As stated in the Introduction, in other test programs these ICD's reduced inflow disturbances and, consequently, tone noise caused by rotor/inflow disturbance interaction. To demonstrate that the ICD acts the same on the QCGAT engine, the SPL spectra from the wall acoustic transducer at the inlet throat are shown in Fig. 10. For these data the engine was tested with all the acoustic panels installed, then tested again with the panels covered with aluminum tape to form hardwall ducts. The spectra illustrate that the ICD reduced the BPF_F tone for both the hardwall and suppressed engine configuration, but did not significantly change other features of the spectra.

The effect of the ICD on the narrowband acoustic spectra at the 50-degree far-field microphone is shown in Fig. 11 for the engine with hardwall ducts. For each engine power setting the spectra with and without ICD No. 1 installed are very similar, except for the BPF_F tone reduction with the ICD (same as noted in the previous figure). The BPF_F and broadband SPL levels taken from spectra at all the far-field microphones, corrected as described in the "Instrumentation and

Data" section, are shown in directivity patterns in Fig. 12. These patterns show that the BPF_F tone was reduced everywhere in the far field with the ICD. For the hardwall tests, these data demonstrate that the far-field tone was dominated by tone from the rotor/inflow disturbance interaction source. This source radiated strongly from both the inlet and exhaust nozzle, as indicated by the large reduction in both the forward and aft quadrants with the ICD installed. When the rotor/inflow disturbance interaction source is absent, as with the ICD installed, some relatively strong tones persisted, indicating that other sources were still present. The various sources and their directivity patterns are discussed further in the next section of this paper.

For the tests with active acoustic panels, the ICD reduced the BPF_F tone in the forward quadrant about the same as for the hardwall configuration. In the aft quadrant, the panels in the bypass duct by themselves reduced tone from all sources, including rotor/inflow disturbance interaction, so the ICD appeared to have small effect.

In addition to the tone noise reduction, the presence of the ICD reduced the broadband noise noticeably in the forward quadrant, particularly at "take-off" power. A similar result was noted in Ref. 11, but not in Refs. 3, 4, and 12. For example, Ref. 3 reported outdoor tests of an engine exhausting into a large muffler, and it was shown that the broadband noise was not changed from engine-alone values when any of four different ICD's was installed on the engine. The far-field spectral data from anechoic chamber fan tests in Refs. 4 and 12 also show little change in broadband level when an ICD is installed. These results suggest that broadband noise on some fans, such as the QCGAT fan, is somehow dependent on incoming turbulence level.

ICD Comparison - The forward quadrant BPF_F and broadband directivity patterns for both ICD's are presented in Fig. 13. These data were obtained with hardwall inlet duct and all acoustic suppression panels active in the aft bypass duct. At the "low" power setting no BPF_F tone lobes are observed for ICD No. 1, while there is a lobe peaking at 50 degrees from a mode just above cut-off for ICD No. 1A. Both ICD's performed the same at angles near the inlet axis.

At "approach" power, both ICD's reveal a lobe, peaking at about 50 degrees, from a mode near cut-off. The lobe noted for ICD No. 1A at "low" power has theoretically moved to a more forward angle, but in the data it seems to have disappeared beneath the stronger tone levels radiated from other combined sources.

At "take-off" power both ICD's indicated the presence of the rotor-alone tone, which is just cut-on at this power setting and tends to propagate toward the sideline. This tone was a little stronger with ICD No. 1. ICD No. 1 also shows stronger tone near the inlet axis, indicating the presence of well-cut-on propagating modes.

The forward broadband directivity patterns at BPF_F (Fig. 13) are the same for both ICD's at all the engine power settings. In Fig. 14, the same result is found over a large range of frequencies. This figure shows the broadband patterns at 0.4 BPF_F and 1.4 BPF_F. The pattern shapes change at "take-off" power. This is a characteristic of rotor speed rather than the frequency at which the broadband SPL is evaluated, as illustrated by comparison of the pattern shapes for "take-off" power (Fig. 13(c)) and "approach" power (Fig. 14(b)) at the same frequency (about 5000 Hz). At "take-off" power the shape changes appear to be characterized mostly by increase in level at sideline angles.

Comparison of data in Refs. 3 and 4 shown that ICD No. 1A sometimes produced greater reduction in BPF_F tone than ICD No. 1. However, the referenced tests were performed with different fans in different facilities, so the residual tone levels may have depended on source differences not related to inflow disturbances, and therefore not controllable with an ICD. The design differences in ICD No. 1A were intended to make distortion levels at the fan even lower than attained with ICD No. 1. The results presented herein for the QCGAT engine did not demonstrate conclusively the effectiveness of these changes, because the acoustic performance of both ICD's No. 1 and No. 1A were about the same. Similar results are discussed in Ref. 12.

Qualitative Analysis of Far-Field Fan Noise Directivity Patterns

Analytical background - In this discussion, far-field fan noise is considered to be made up of single-mode and multimodal acoustic radiation. Single-mode radiation refers to a spinning acoustic mode from a single engine source involving the fan (e.g., rotor/strut interaction noise). Only single modes at BPF_F will be considered herein. The radiation patterns for single modes, which are lobe shaped and peak at a level called SPL_{max}, were determined with a computer program for the exact Wiener-Hopf solution[13] because the program was readily available. Computations were made for the case of flow everywhere, then corrected to the case of zero external flow using the technique in Ref. 14.

Multimodal radiation refers to the combined noise from all propagating modes, with no dominant single mode. Examples of multimodal radiation are broadband noise and noise from rotor interaction with random inflow disturbances (e.g., turbulence). In this paper, the term "inflow disturbances" means incoming turbulence plus any other random or steady inflow distortions. Only distortions which are random in time or space can produce multimodal radiation. For forward radiated multimodal noise, the "approximate" analytical expressions in Ref. 13 were used. Although called "approximate," the reference shows the closed form expressions to be accurate for equal-power-per-mode noise. The directivity patterns are of the form

$$SPL = SPL_{max} + 10 \log[\cos \psi \sin^n \psi], \text{ dB} \quad (1)$$

where ψ is the angle from the engine inlet axis. SPL_{max} occurs when $\psi = \tan^{-1}\sqrt{n}$. Increasing the exponent n serves to shift acoustic power away from an equal power per mode ($n = 0$) pattern peaking on the axis toward a power

distribution weighted toward cut-off modes for which the pattern peaks nearer the sideline. A value of $n = 1/2$ gave overall best match for the QCGAT engine data and was used to calculate the analytical directivity patterns in this report.

For aft radiated multimodal noise the approximate expressions in Ref. 7 were used. These expressions resulted from an initial effort at analysis of this kind of noise. They are based on equal-power-per-mode concepts, and are shown in the reference to be accurate compared to an exact solution for angles from the exhaust nozzle axis up to about 30 degrees from the inlet axis. The directivity patterns are of the form

$$SPL = SPL_{max} + 10 \log[M_D + (1 - M_D^2)\cos(180^\circ - \psi)], dB \qquad (2)$$

where M_D is the exhaust nozzle flow Mach number. This expression can be used only outside the zone of relative silence. The forward boundary of this zone, ψ_{ZS}, is given by

$$\psi_{ZS} = 180^\circ - \cos^{-1}\left(\frac{1}{1 + M_D}\right), \text{ deg} \qquad (3)$$

where ψ_{ZS} is measured from the inlet axis.

In common with other radiation pattern analyses, the analyses used herein do not predict absolute SPL level, but rather give the relative level referred to some arbitrary maximum, SPL_{max}.

In the remaining parts of this section the analytical patterns will be superimposed on plots of various far-field directivity patterns. This type of qualitative comparison gives good insight into the engine sources contributing to the far-field noise.

Rotor/inflow disturbance interaction tone - The directivity patterns for the engine with hard-wall ducts and without an ICD, previously shown in Fig. 12, are dominated by rotor/inflow disturbance interaction tone, which is multimodal in this engine. The same data are shown again in Fig. 15. The analytical multimodal directivity patterns, calculated as described in the preceding part of this section, are also shown with SPL_{max} arbitrarily chosen so that the total (forward plus aft) patterns best match the data. Considering only the BPF_F parts of the figure, the match thus found is very good everywhere at "approach" power. At "take-off" power the match is reasonably good, but at the sideline and in the aft quadrant the aft analytical curve shape is too flat. This discrepancy might be caused by any of several factors: (1), the calculated effective exhaust nozzle Mach number may be too high because of the assumed perfect mixing, thus leading to high analytical levels as calculated by Eq. (2); (2), the power in the modes near cut-off (which tend to propagate to the sideline and forward from the nozzle) may be less than assumed in the equal-power-per-mode analysis because the modes near cut-off may have been cut-off in the long aft duct (see section entitled "Cut-Off Speeds"); and (3), some other important considerations may not yet be included in the multimodal analysis.

The experimental tone level fell suddenly in the zone of relative silence. The analysis predicts no power (SPL = 0) in this zone, so the analysis qualitatively predicts the correct result.

In summation, the approximate multimodal expressions match most features of the rotor/inflow disturbance BPF_F directivity pattern. The least agreement occurs at "take-off" power at the sideline and in the aft quadrant where the aft analytical pattern shape is too flat.

Broadband noise - Consider now the broadband portions of Fig. 15. The analytical multimodal directivity patterns are the same as for the rotor/inflow disturbance interaction tone discussed in the preceding part of this section, only with SPL_{max} shifted to different arbitrary levels for best matches with the broadband data. At "approach" power the match is good in the forward quadrant, but agreement becomes less when the aft radiated noise is included because the aft analytical curve shape is too flat to satisfy both the sideline data and the measured peak at 110 degrees. Possible causes for the discrepancy are the same as discussed in the preceding part for BPF_F tone at "take-off" power.

For the broadband noise at "take-off" power the situation is similar, but agreement between the analytical patterns and the data is poorer. At this fan speed, forward and aft pattern shapes set at several different SPL_{max} could be used to compare with the data. None match the total measured directivity pattern very well. The broadband patterns shown in Fig. 15(b) were chosen to preserve the influence of aft radiated noise at forward angles, as was implied in the discussions of Figs. 7 and 14. On this basis, the aft pattern does not match the data at aft angles, and appears to miss completely the local SPL peak at 110 degrees. For both power settings, the broadband noise fell off gradually into the zone of relative silence. This behavior is not the same sudden drop noted for the BPF_F tone, but has been observed in data from other acoustic tests.[7]

In summation, the multimodal analytical radiation expressions match well with the experimental data for broadband noise measured near BPF_F frequency in the forward quadrant at the "approach" power setting, but not in the aft quadrant at either power setting. These discrepancies are similar to those noted for the BPF_F multimodal tone data.

Engine tone sources with ICD - In this part of the paper the far-field directivity patterns will be searched for evidence of propagating single modes that leads to identification of their sources. Modes are best identified just after they become cut-on (i.e., begin to propagate to the far field), by a lobe which peaks near 50 to 60 degrees from the inlet axis. The exact angle is found from single-mode analytical radiation patterns. When a lobe is found just cut-on at any given fan speed, the mode number can be determined with the aid of Fig. 8; the probable source then can be identified from the mode number and engine configuration. The exercise is here limited to forward noise only, and makes use of the Wiener-Hopf analytical program with radiation angles adjusted for no external flow, as described in a

previous part of this section. The directivity patterns examined are for the engine with ICD No. 1, hardwall inlet duct, and all acoustic panels in the bypass duct. This configuration was chosen because the forward-quadrant fan noise is least attenuated in the inlet, and least contaminated by rotor/inflow disturbance interaction noise or noise radiated from the aft end.

The patterns for both broadband and BPF_F tone are given in Fig. 16. The broadband patterns are not directly involved in mode identification, but are helpful in judging appropriate levels for the other analytical patterns. In the tone patterns, the search will be confined to single modes having lobe numbers of $m = 4$, 12, 20, 24, 28, and 36 only. These are the modes most likely to be generated during the tests (see section entitled "Cut-Off Speeds") because modes from rotor/stator interaction are cut-off by high vane/blade ratios. For these modes side lobes radial orders greater than the first, and modal cancellation due to phase difference in the far field, all are ignored.

The search procedure consists of matching analytical pattern shapes to measured directivity patterns. As the first example, the matches obtained at the lowest engine power setting are shown in Fig. 16(a). The analytical multimodal tone pattern, arbitrarily set a few dB above the broadband pattern, represents the residual multimodal BPF_F tone. The residual tone is the far-field sum of tone noise from all propagating random sources in the engine, including any rotor/inflow disturbance interaction tone that has not been removed by the ICD. The patterns from the $m = 4$ and $m = 12$ single modes, the only ones of interest cut-on at this speed, are added to the multimodal pattern so that the total analytical pattern shape (shown by the dot-dash line) gives a reasonable match with the measured data. The pattern thus constructed suggests that the $m = 4$ mode, which comes from a rotor/strut interaction source, propagated strongly. However, it may be only one of several well-cut-on modes which held up the tone SPL level near the axis. On the other hand, the $m = 12$ mode, which can come from both rotor/strut and rotor/ICD rib interaction, is fairly weak as indicated by the absence of any obvious lobe in these data near 60 degrees. (In Fig. 12, a lobe from the $m = 12$ mode, which is just cut-on at this speed, can be seen in the data for ICD No. 1A).

The search for single-mode sources is continued by constructing analytical patterns at higher speeds to "take-off" power. The broadband SPL_{max} level is increased by an amount calculated by

$$\Delta SPL_{max} = \frac{1}{2}\left\{50 \log \frac{M_R}{(M_R)_{ref}} + 1.7(A - A_{ref})\right\}, \text{ dB} \qquad (4)$$

where M_R is the tip relative Mach number, A is the tip relative flow angle (deg), and the subscript "ref" refers to a reference level (taken here as the lowest speed tested). The portion of the equation in the outermost brackets is based on broadband correlations for other fans, in Refs. 16 and 17. The multiplier 1/2 is required to make the equation fit the QCGAT broadband results, but no reason is known why it is needed. To maintain order the calculated ΔSPL_{max} is also used to increase the multimodal BPF_F tone and single-mode pattern levels, although correlations are not available to justify this application.

At the next higher fan speed, Fig. 16(b), the analytical BPF_F tone patterns constructed as described are much lower than the measured data at forward angles. As previously noted, several well-cut-on but unidentified modes seem to be holding up the tone SPL level near the axis. The same trend can be seen in many of the following figures.

At "approach" power, Fig. 16(c), a well defined lobe from a just-cut-on mode appeared near 60 degrees. This lobe comes from the $m = 20$ mode, which is generated by a rotor/strut interaction source.

At medium power settings, Figs. 16(d) and (e), lobes from $m = 24$ and $m = 28$ modes can be seen. The sources for these modes are rotor/ICD rib and rotor/strut interaction, respectively. The $m = 28$ mode seems to be the stronger of the two.

At "take-off" power, Fig. 16(f), lobes from all modes which became cut-on at lower fan speeds are bunched together near the axis. The SPL level is high, but individual lobes are not distinguishable in the data. The mode from the rotor-alone pressure field, $m = 36$, is cut-on at this fan speed (see Fig. 8), and accounts for much of the tone near the sideline. However, SPL_{max} for this tone, as well as others at the higher fan speeds, seems to be analytically predicted closer to the inlet axis than measured by the data. The reason, if this is true, is not known.

The data plotted in Fig. 16 show that the broadband noise analytical pattern shapes agree well with the measured data except at "take-off" power. The same discrepancy was noted in the discussion of Fig. 15.

In summation, comparisons of the forward-quadrant analytical and measured directivity patterns, although qualitative, showed that this engine produced residual mulitmodal BPF_F tone noise at all speeds, as well as rotor/strut interaction and rotor-alone tone noise at speeds where modes from these sources were cut-on. Some rotor/ICD rib interaction tone noise was detected but was not strong enough to distort patterns attributable to engine-only sources.

Summary of Results

The AiResearch QCGAT engine was tested on an outdoor test stand with two inflow control devices (ICD's) which were available from previous test programs, and with three inlet lips. The previous test programs had demonstrated that both ICD's reduced rotor/inflow disturbance interaction tone noise. For some of the QCGAT tests, the acoustic suppression panels in the inlet or in the bypass duct were covered with aluminum tape to form hardwall ducts having the same size and configuration. The tests were performed to compare the acoustic effects of the ICD's and the lips on the

same engine, and to compare far-field directivity patterns calculated by applicable existing analyses with the measured BPF_F and broadband patterns.

When an ICD was installed on the engine with hardwall ducts the BPF_F tone was found to be reduced significantly everywhere in the far-field. These data showed that rotor/inflow disturbance interaction tone dominated the far-field noise, and was radiated strongly from the inlet and exhaust nozzle. For the same ICD on the engine with active acoustic panels, tone reduction in the forward quadrant was comparable to the reduction measured in the hardwall tests; however, in the aft quadrant all tone noise was attenuated so much by large acoustic panels in the bypass duct that the ICD appeared to have small effect. The broadband noise also was reduced slightly when the ICD was installed. The same reduction was noted on one previous test program but not on several others; the reason for reduction is not known.

Both of the ICD's were built with the same size honeycomb, and had the same overall size and shape. The tests to compare performance of the ICD's with hardwall inlet ducts showed only minor differences in the BPF_F directivity patterns. Broadband noise was the same for both ICD's.

The inlet lips were tested with a hardwall inlet duct. The forward-quadrant BPF_F and broadband directivity patterns were found to be essentially the same for all the lips. This result was expected because the lips were the same except for shape differences outside the highlight.

Comparison of the analytical and measured directivity patterns showed that the simple expressions for multimodal radiation used predict most features of the rotor/inflow disturbance interaction BPF_F pattern. At high fan speeds, the shape of the analytical multimodal tone pattern from the exhaust nozzle was too flat, resulting in noticeable differences between the measured and analytical patterns near the sideline and in the aft quadrant. The same difficulty was noted for the broadband pattern, but the discrepancy between analytical and measured patterns was greater than for tone.

Using an ICD to reduce rotor/inflow disturbance interaction noise, lobes from several propagating single modes were found in the forward-quadrant BPF_F data. From the fan speed at which these lobes first appeared, the sources of these modes were identified to be rotor/strut interaction and the rotor-alone pressure field. Some rotor/ICD rib interaction tone was detected, but the level was low.

References

1. Morgren, W. M., Blackmore, W. L., Davis, F. G., Hale, P. L., Kisner, L. S., Steele, M. A., and Thompson, C. E., "Test Report QCGAT Engine and Engine/Nacelle Systems," AiResearch Manufacturing Company, Phoenix, AZ, AIRESEARCH-21-3070, June 15, 1979.
2. General Aviation Propulsion, NASA CP-2176, 1980.
3. McArdle, J. G., Jones, W. L., Heidelberg, L. J., and Homyak, L., "Comparison of Several Inflow Control Devices for Flight Simulation of Fan Tone Noise Using a JT15D Engine," NASA TM-81505, 1980.
4. Ho, P. Y., Smith, E. B., and Kantola, R. A., "An Inflow Turbulence Reduction Structure for Scale Model Fan Testing," AIAA Paper 79-0655, Mar. 1979.
5. Morgren, W. M., et al., "Final Design Report QCGAT Engine Program," AiResearch Manufacturing Company, Phoenix, AZ, AIRESEARCH-21-2474(2), Dec. 15, 1978.
6. Rice, E. J., "Inlet Noise Suppressor Design Method Based Upon the Distribution of Acoustic Power with Mode Cutoff Ratio," Advances in Engineering Science, NASA CP-2001, Vol. 3, 1976, pp. 883-894.
7. Rice, E. J., and Saule, A. V., "Far-Field Radiation of Aft Turbofan Noise," NASA TM-81506, 1980.
8. Mathews, D. C., and Nagel, R. T., "Inlet Geometry and Axial Mach Number Effects of Fan Noise Propagation," AIAA Paper 73-1022, Oct. 1973.
9. Lansing, D. L., Dreschler, J. A., and Pusey, C. G., "Radiation of Sound From an Unflanged Circular Duct with Flow," 79th Meeting, Acoustical Society of America, April 21-24, 1970, Session D, Paper 5.
10. Beckemeyer, R. J., Sawdy, D. T., and Garner, P., "Computational Methods for Acoustic Radiation from Circular Ducts," AIAA Paper 75-516, Mar. 1975.
11. Woodward, R. P., Wazyniak, J. A., Shaw, L. M., and MacKinnon, M. J., "Effectiveness of an Inlet Flow Turbulence Control Device to Simulate Flight Fan Noise in an Anechoic Chamber," NASA TM-73855, 1977.
12. Woodward, R. P., and Glaser, F. W., "Effect of Inflow Control on Inlet Noise of a Cut-On Fan," AIAA Paper 80-1049, June 1980.
13. Savkar, S. D., and Edelfelt, I. H., "Radiation of Cylindrical Duct Acoustic Modes with Flow Mismatch," General Electric Co., Schenectady, NY, SRD-75-029, Mar. 1975. (NASA CR-132613.)
14. Heidmann, M. F., Saule, A. V., and McArdle, J. G., "Analysis of Radiation Patterns of Interaction Tones Generated by Inlet Rods in the JT15D Engine," AIAA Paper 79-0581, Mar. 1979.
15. Rice, E. J., "Multimodal Far-Field Acoustic Radiation Pattern - An Approximate Equation," AIAA Paper 77-1281, Oct. 1977.
16. Ginder, R. B., and Newby, D. R., "A Study of Factors Affecting the Broadband Noise of High-Speed Fans," AIAA Paper 76-567, July 1976.
17. Gliebe, P. R., "The Effect of Throttling on Forward Radiated Fan Noise," AIAA Paper 79-0640, Mar. 1979.

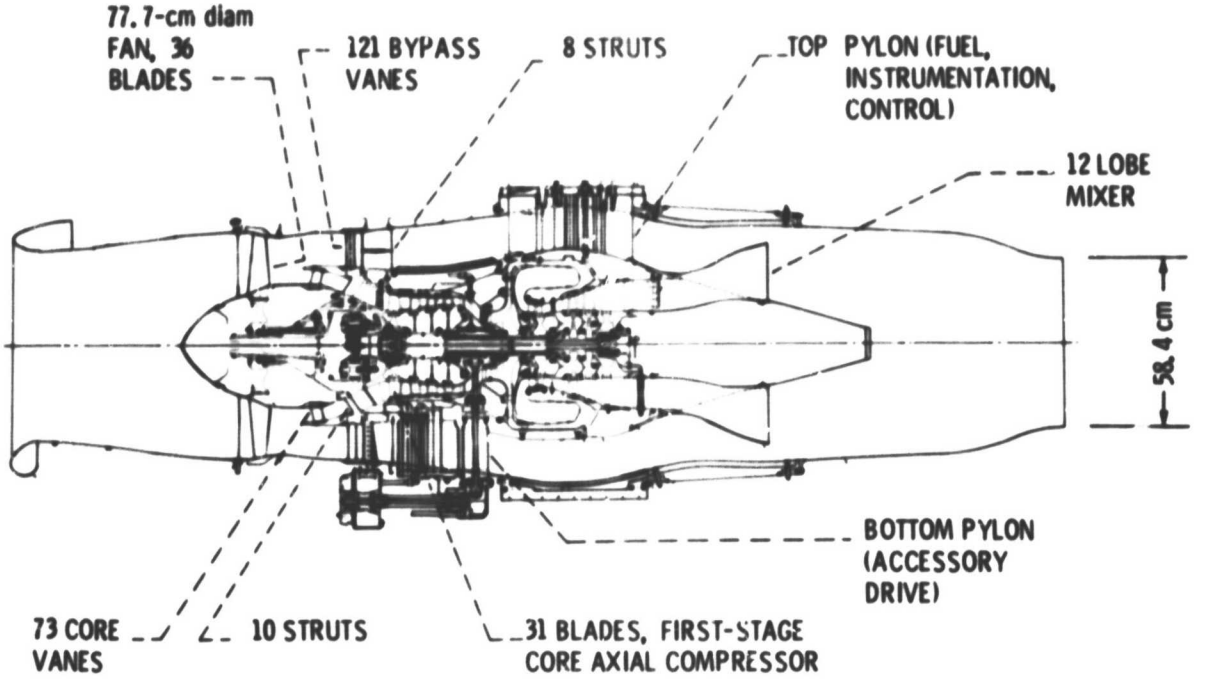

(a) CROSS-SECTION SKETCH.

(b) ENGINE ON VLF TEST STAND.

Figure 1. - AiResearch QCGAT engine with "flight simulator" inlet lip.

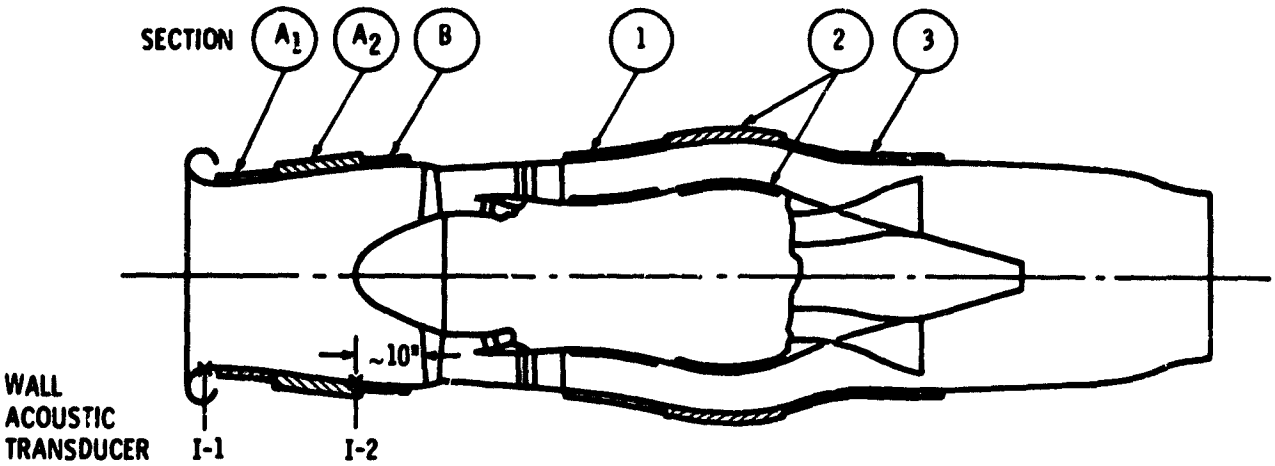

PARAMETER	INLET DUCT		FAN EXHAUST		
	SECTION A	SECTION B	SECTION 1	SECTION 2	SECTION 3
AVERAGE DUCT HEIGHT, h, in.[1]	13.8	15.1	5.7	5.6	6.7
PANEL (A_1 and A_2) LENGTH, in.	17.6	6.0	12.6	15.3	20.8
TUNED CENTER FREQUENCY, Hz	1000 1000	2500	2500	4000	2000
CAVITY DEPTH, INCHES	1.1 0.72	0.52	0.56	0.36	0.77
PERCENT OPEN AREA	8.6 5.8	14.2	7.0	8.6	6.8
FREQUENCY PARAMETER, fH/C^2	2.131 1.99	5.644	2.05	1.59	1.92
CONDITION TUNED FOR:	SIDELINE	SIDELINE	APPROACH	APPROACH	APPROACH

[1]FOR INLET h = D/2 [2]FOR ONE WALL TREATED, H = 2h

Figure 2. - QCGAT acoustic suppression panels.

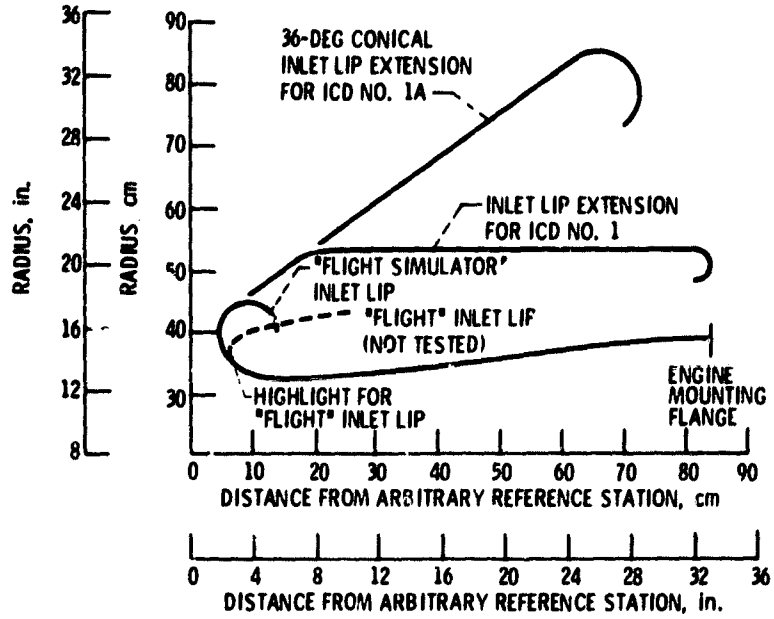

Figure 3. - Cross-section shape of inlet and lips for AiResearch QCGAT engine.

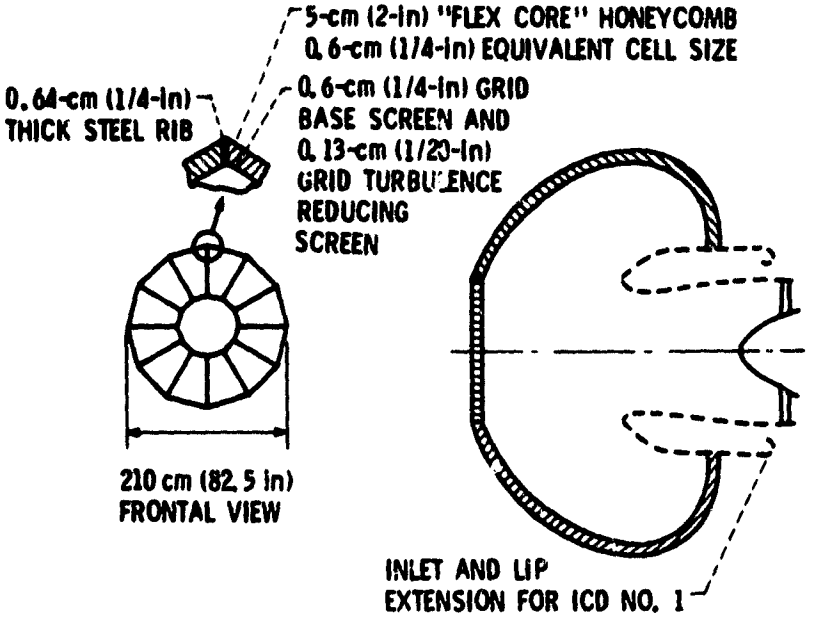

(a) ICD No. 1.

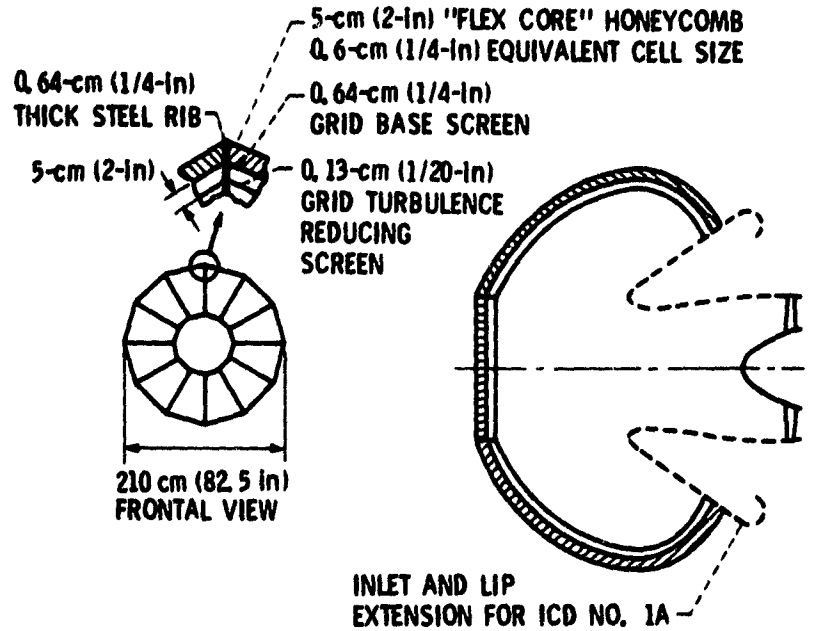

(b) ICD No. 1A.

Figure 4. - Inflow control device configurations.

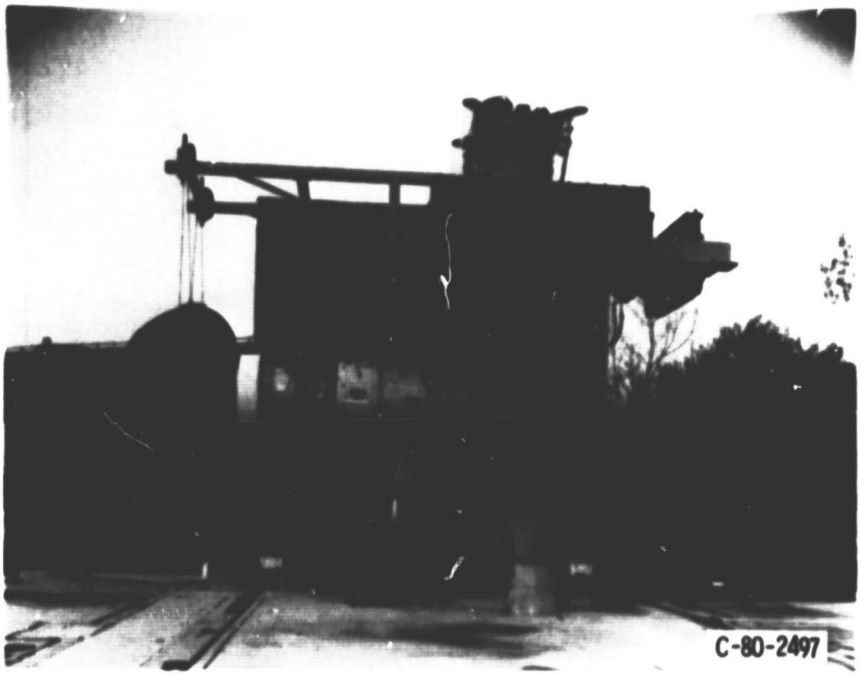

(c) ICD NO. 1 MOUNTED ON ENGINE.

Figure 4. - Concluded.

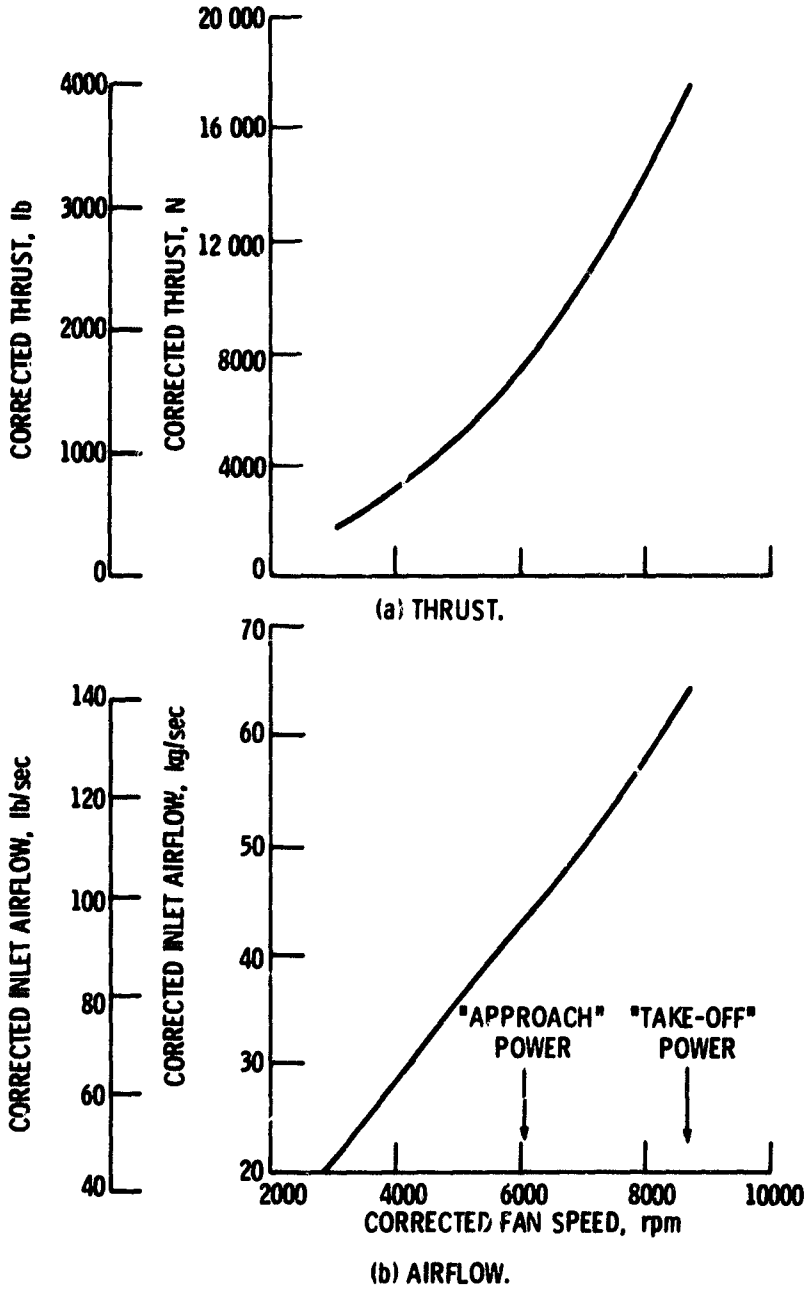

Figure 5. - Engine aerodynamic performance with mixer exhaust system.

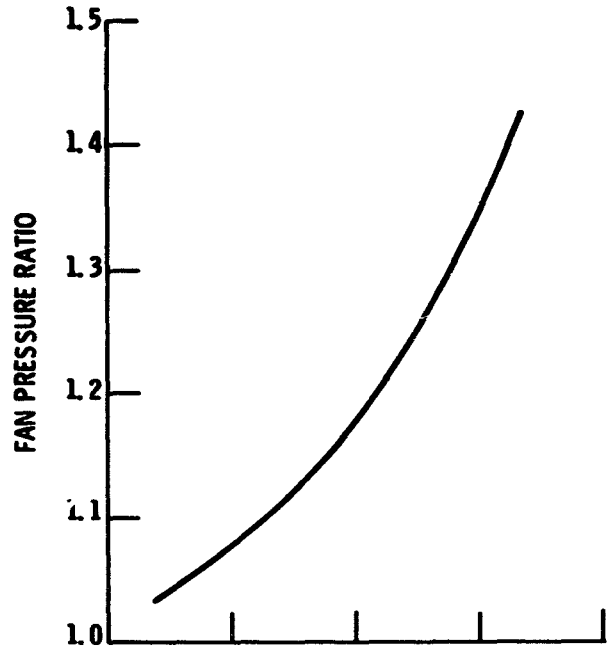

(c) FAN PRESSURE RATIO.

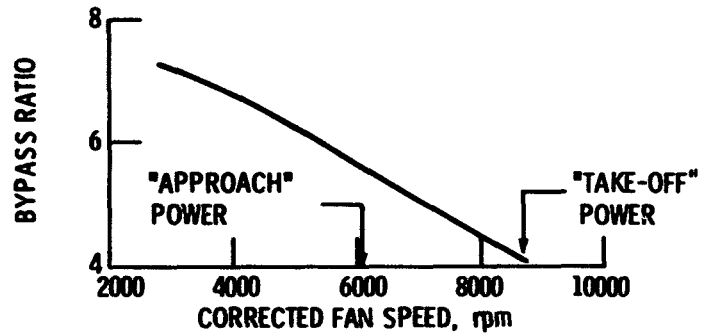

(d) BYPASS RATIO.

Figure 5. - Concluded.

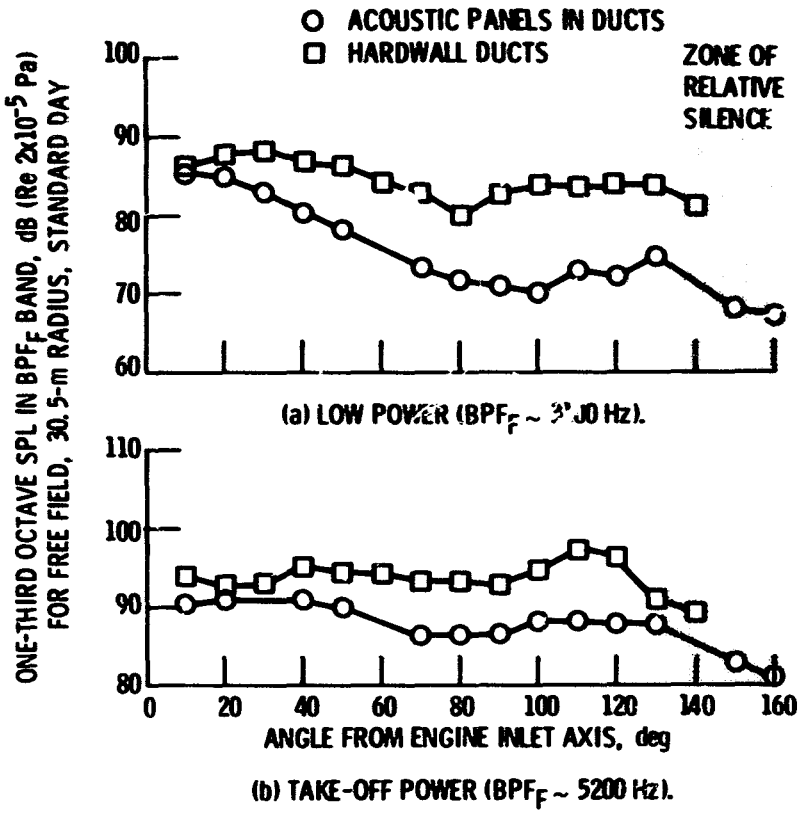

(a) LOW POWER (BPF$_F$ ~ 3700 Hz).

(b) TAKE-OFF POWER (BPF$_F$ ~ 5200 Hz).

Figure 6. - Directivity patterns for engine with flight simulator inlet lip, no ICD.

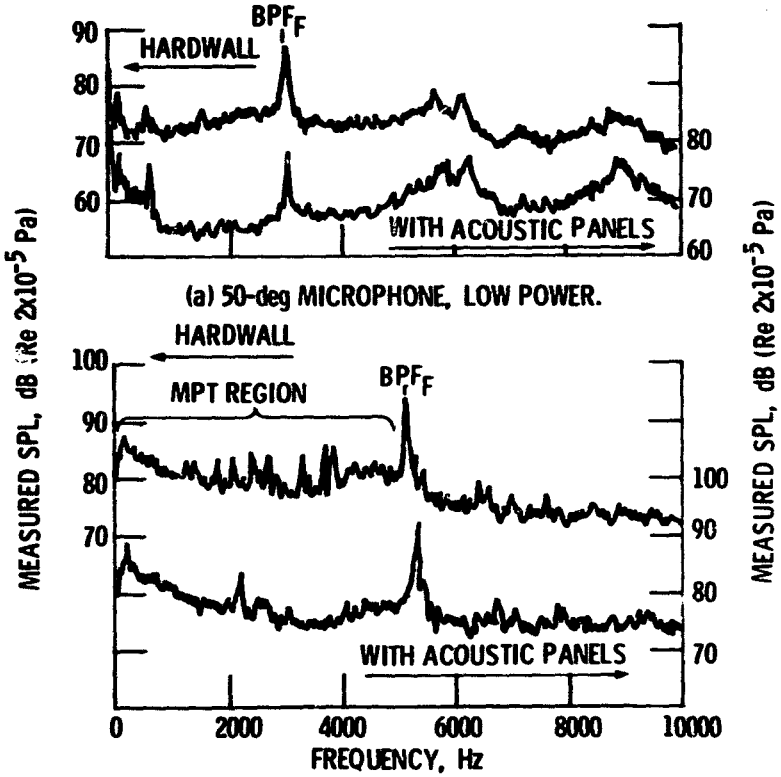

(a) 50-deg MICROPHONE, LOW POWER.

(b) 50-deg MICROPHONE, "TAKE-OFF" POWER.

Figure 7. - Far-field microphone spectra for engine with flight simulator lip, no. ICD. Analyzer bandwidth 25 Hz.

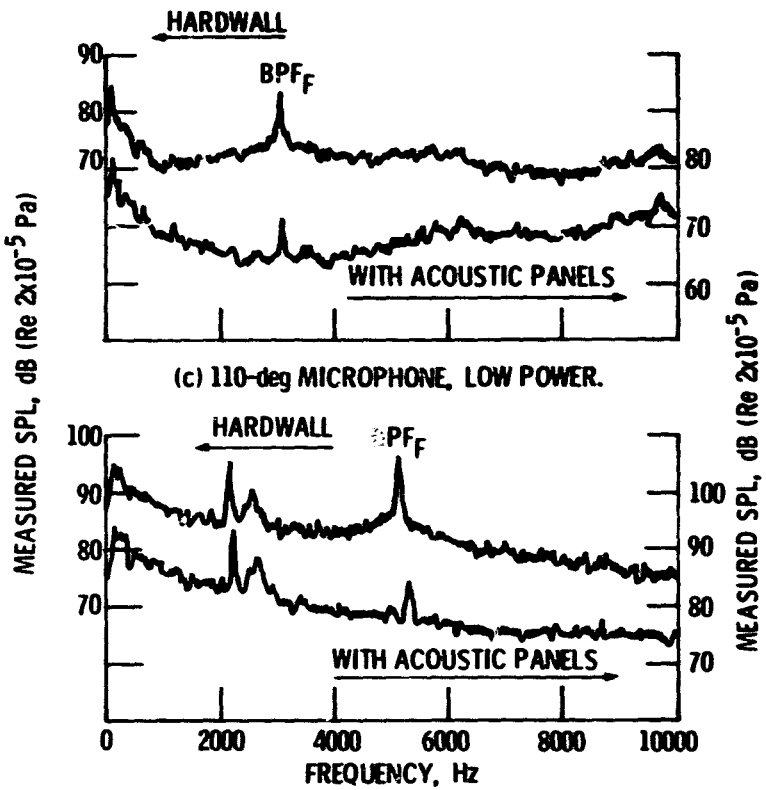

(c) 110-deg MICROPHONE, LOW POWER.

(d) 110-deg MICROPHONE, "TAKE-OFF" POWER.

Figure 7. - Concluded.

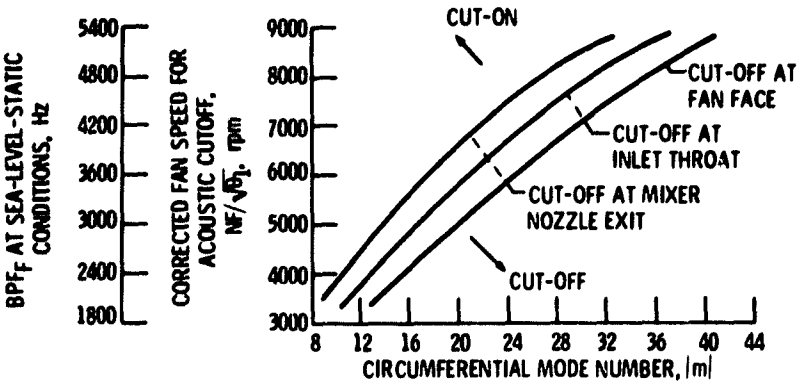

(a) MODE CUT-OFF SPEEDS FOR FAN FUNDAMENTAL TONE.

Figure 8. - Acoustic modes in QCGAT engine for 0th (first) radial order. "Take-off" power at 8700 rpm; "approach" power at 6020 rpm.

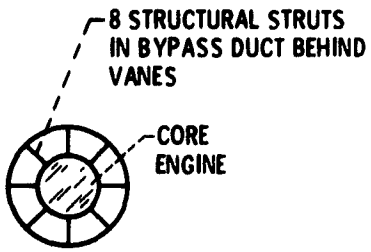

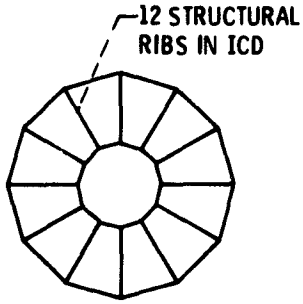

FOR 36 FAN BLADES AND 8 ENGINE STRUTS, $m = 36 - 8K$

K = 0	m = 36 (ROTOR ALONE)
1	28
2	20
3	12
4	4
5	-4
6	-12
ETC.	

FOR 36 FAN BLADES AND 12 RIBS, $m = 36 - 12K$

K = 0	m = 36 (ROTOR ALONE)
1	24
2	12
3	0 (PLANE WAVE)
4	-12
5	-24
ETC.	

(b) CIRCUMFERENTIAL MODES MOST LIKELY TO BE PRODUCED.

Figure 8. - Concluded.

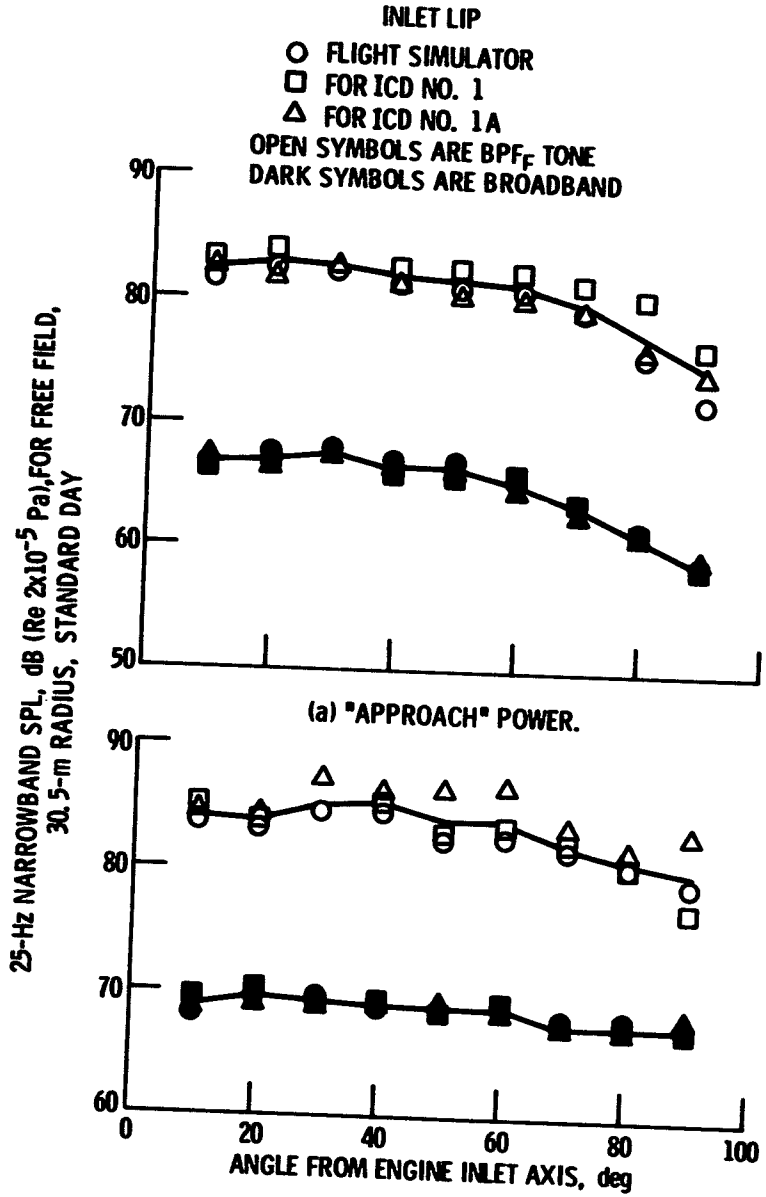

Figure 9. - Comparison of forward-quadrant directivity patterns for three inlet lips. Hardwall inlet duct, acoustic panels in bypass duct, no ICD.

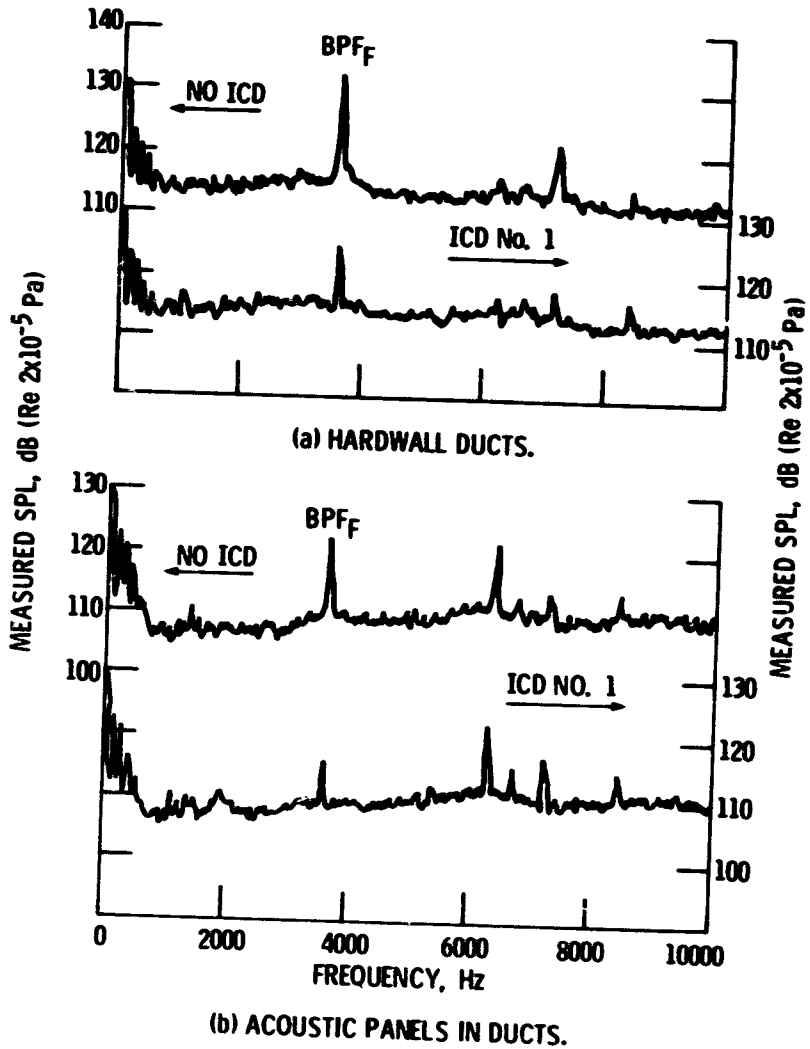

Figure 10. - Effect of ICD on acoustic pressures measured by wall acoustic transducer I-1 at "approach" power, analyzer bandwidth 25 Hz.

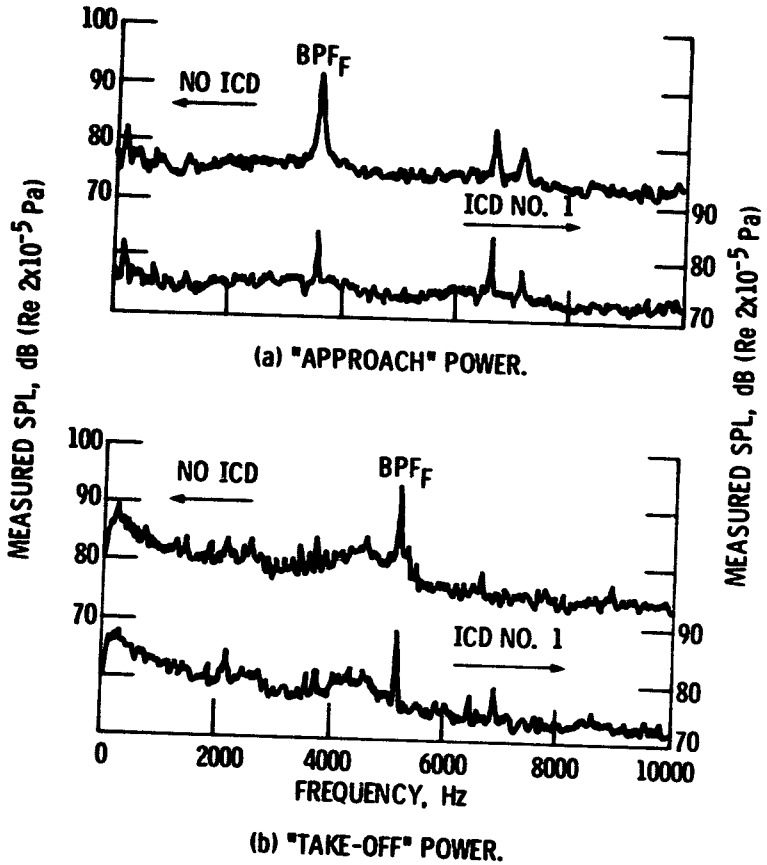

(a) "APPROACH" POWER.

(b) "TAKE-OFF" POWER.

Figure 11. - Effect of ICD on spectra at 50-degree far-field microphone. Hardwall ducts, analyzer bandwith 25 Hz.

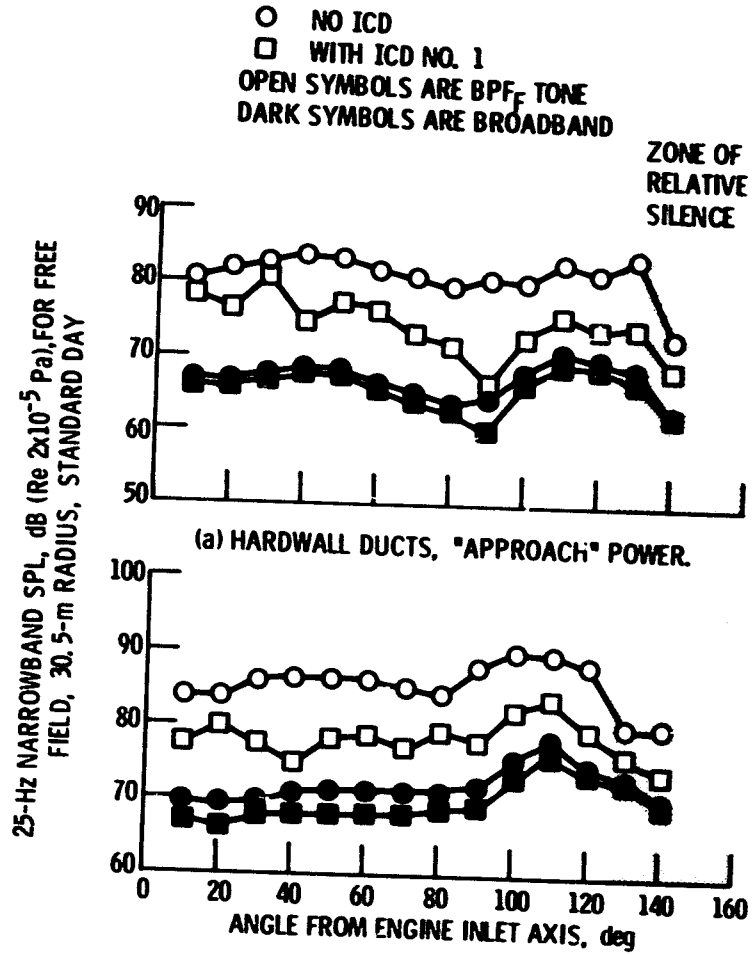

(a) HARDWALL DUCTS, "APPROACH" POWER.

(b) HARDWALL DUCTS, "TAKE-OFF" POWER.

Figure 12. - Effect of ICD on BPF$_F$ tone and broadband directivity patterns.

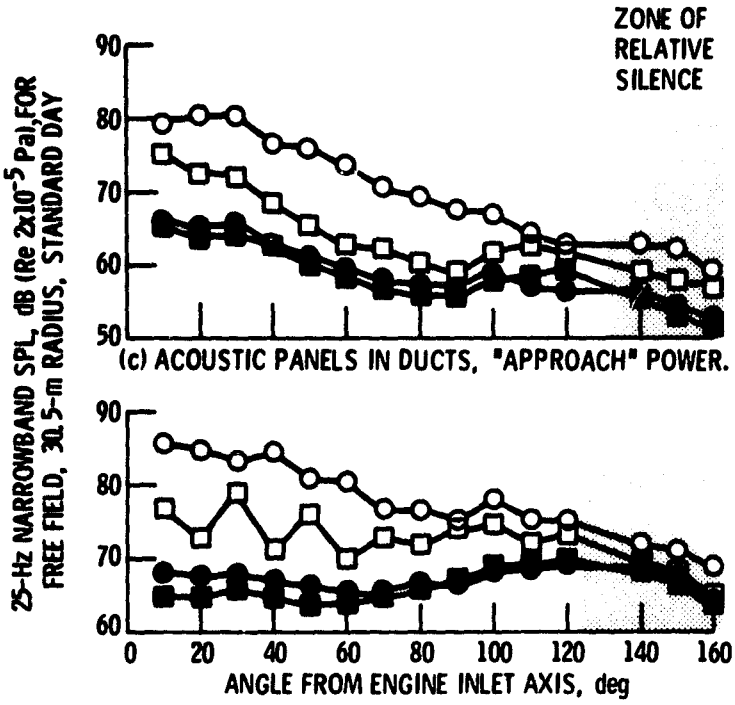

(c) ACOUSTIC PANELS IN DUCTS, "APPROACH" POWER.

(d) ACOUSTIC PANELS IN DUCTS, "TAKE-OFF" POWER.

Figure 12. - Concluded.

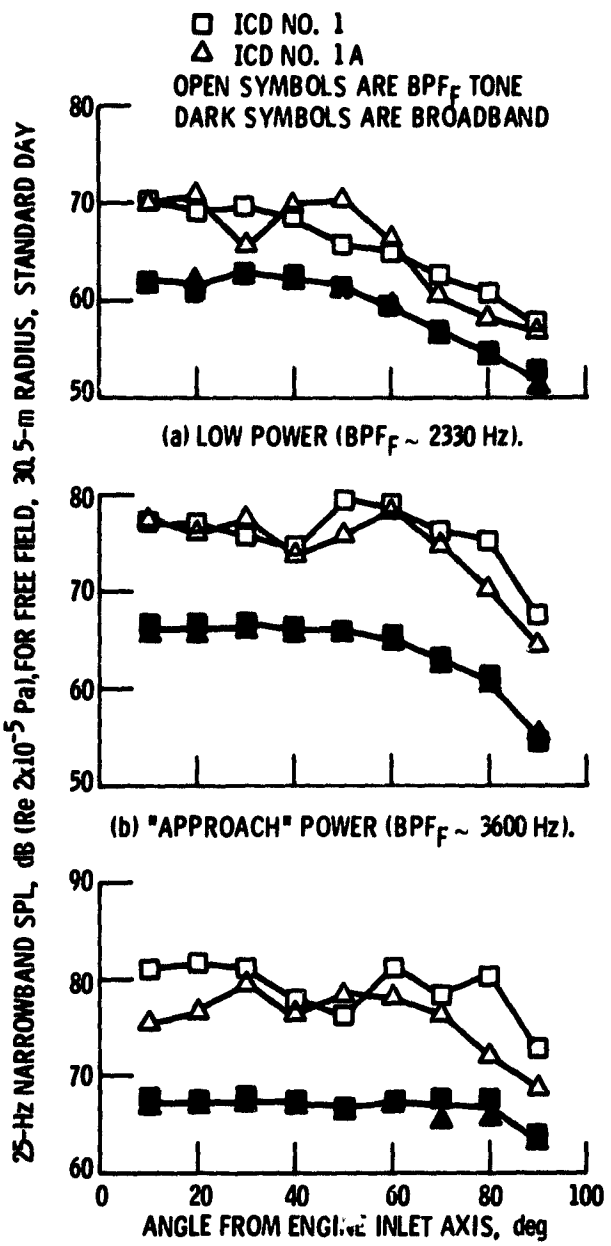

Figure 13. - Comparison of forward-quadrant directivity patterns for both ICD's. Hardwall inlet duct, acoustic panels in bypass duct, mixer exhaust.

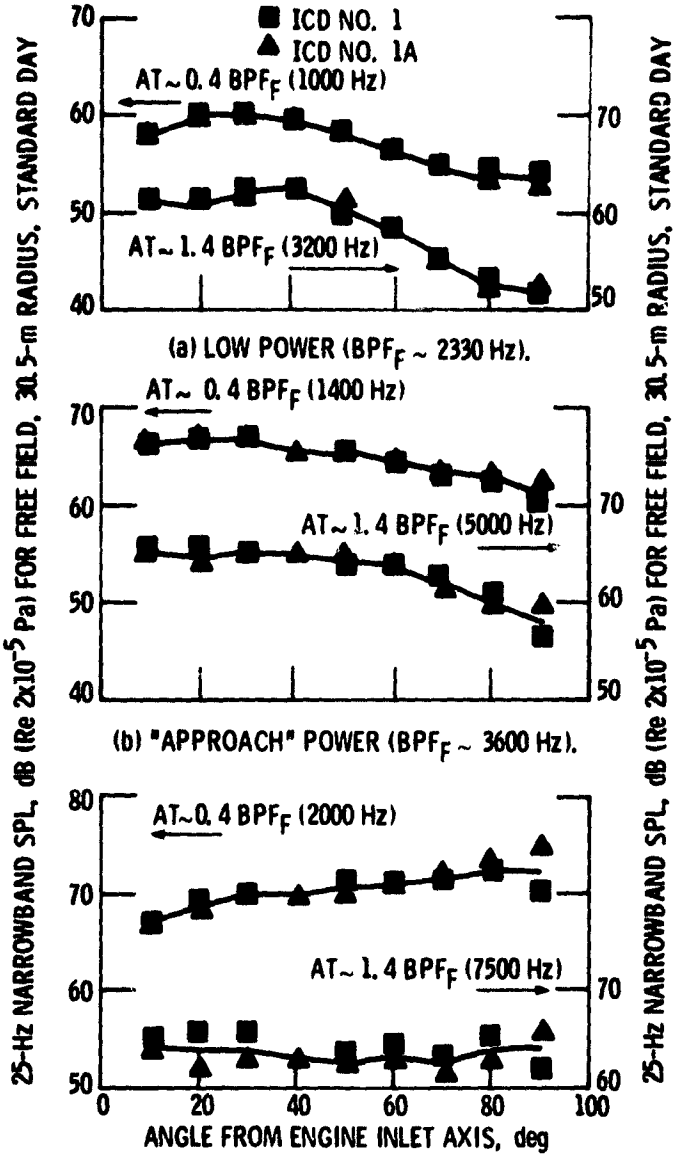

Figure 14. - Comparison of broadband noise for both ICD's evaluated at frequencies above and below BPF$_F$. Hardwall inlet duct, acoustic panels in bypass duct.

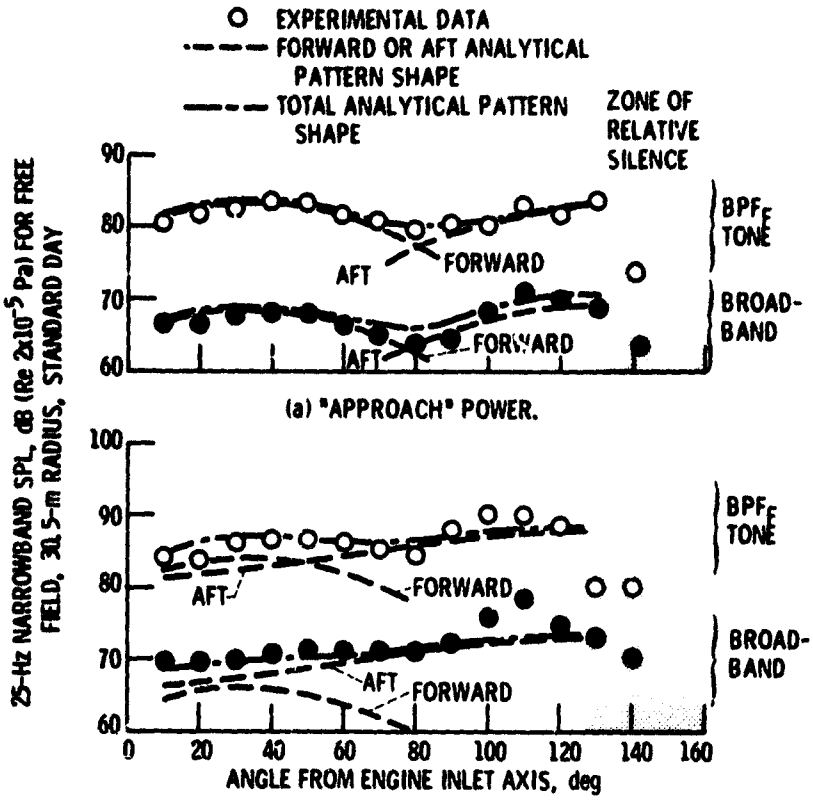

(a) "APPROACH" POWER.

(b) "TAKE-OFF" POWER.

Figure 15. - Qualitative comparison of experimental and analytical directivity patterns. Engine configuration hardwall without ICD. Analytical patterns for multimodal radiation.

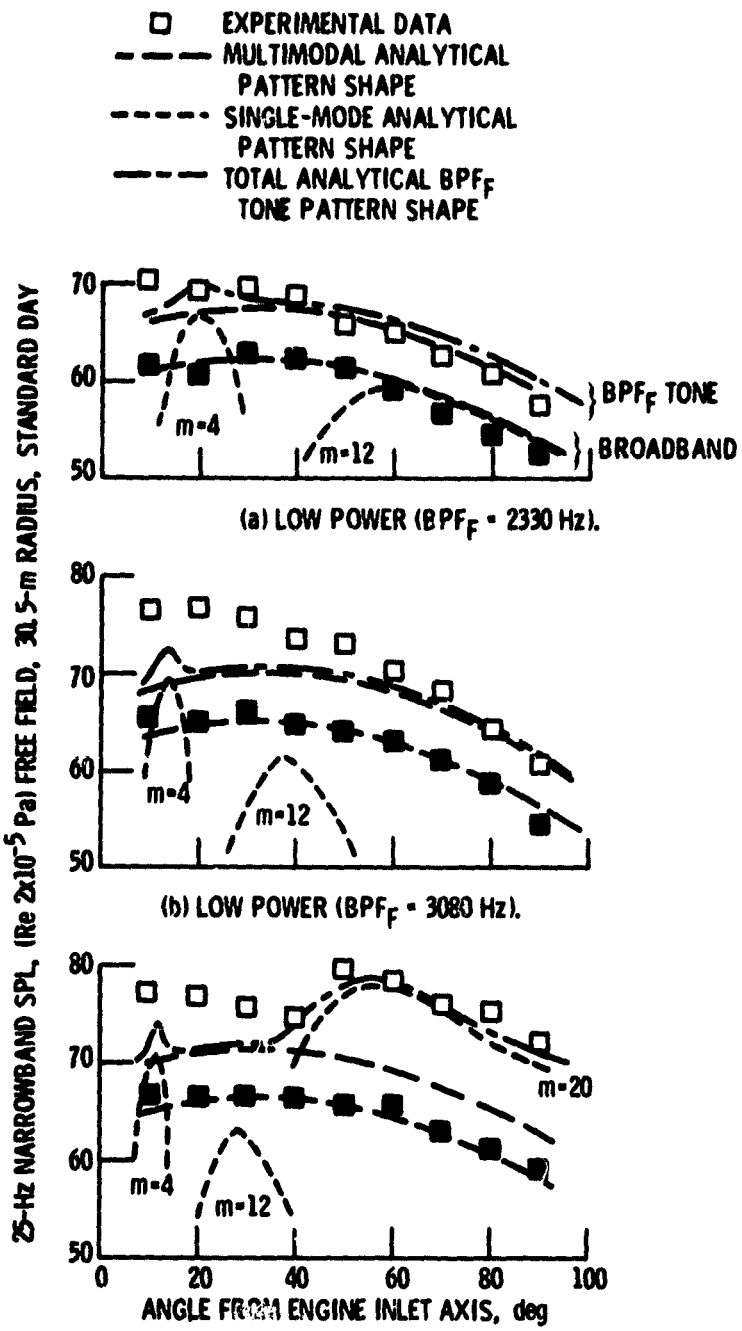

Figure 16. - Qualitative comparison of experimental and analytical forward directivity patterns. Engine with hardwall inlet duct, all acoustic suppression panels in bypass duct.

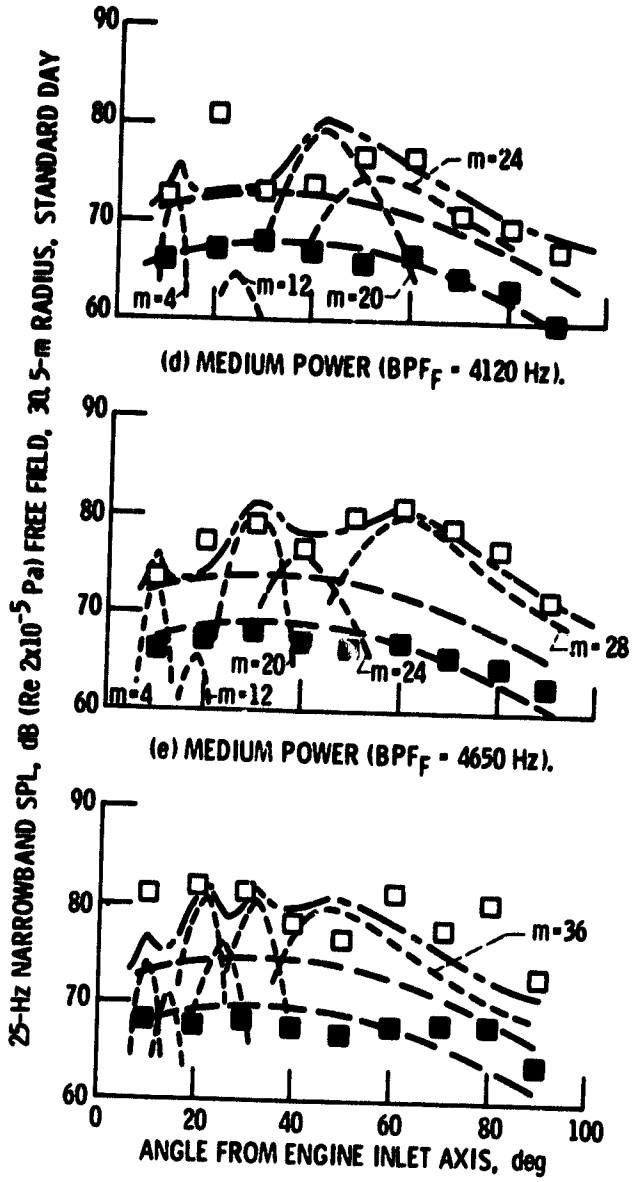

(d) MEDIUM POWER (BPF_F = 4120 Hz).

(e) MEDIUM POWER (BPF_F = 4650 Hz).

(f) "TAKE-OFF" POWER (BPF_F = 5230 Hz).

Figure 16. - Concluded.